Lifetime measurements in ^{206}Po with a shell-model interpretation

V. Karayonchev,[1,2] J. Jolie,[1] D. Bittner,[1] M. Beckers,[1] A. Esmaylzadeh,[1] J. Fischer,[1] C. Fransen,[1] J. Garbe,[1] L. Knafla,[1] C.-D. Lakenbrink,[1] and M. Ley[1]

[1]*Institut für Kernphysik, Universität zu Köln, 50937 Köln, Germany*

[2]*Argonne National Laboratory, Lemont, Illinois 60439, USA*

(Received 13 July 2023; accepted 15 September 2023; published 2 November 2023)

The lifetimes of the first excited 2^+ and 4^+ states in ^{206}Po were measured using the recoil-distance Doppler-shift method. The experimental results were compared to large-scale shell-model calculations that describe the deduced transition probabilities well. Those calculations were extended to the neighboring ^{204,208}Po isotopes giving a good overall description of the yrast states. However, the calculations underpredict the energies of the 6_1^+ and 8_1^+ states, which suggests that further improvement of the proton-neutron interaction is required.

DOI: 10.1103/PhysRevC.108.054302

I. INTRODUCTION

The evolution of the nuclear structure of nuclei when moving away from closed shells is in the focus of both experimental and theoretical nuclear physics. Starting at a closed shell, the nuclear structure is mainly defined by the single-particle motion of the valence nucleons. As both valence protons and neutrons are added, it is well known that the long-ranged proton-neutron quadrupole interaction increases, causing collectivity to develop [1,2]. A simple scaling based on the number of valence protons and neutrons, i.e., the N_pN_n scheme [3], can elegantly describe the evolution of key experimental indicators of collectivity, such as the energy of the first-excited 2^+ state and the $B(E2)$ values, in even-even nuclei. This evolution is usually a smooth process and the underlying shell structure is washed out due to the rapid development of proton-neutron correlations. If one looks, however, at the structural evolution of isotopic or isotonic chains that lie close to a magic number, due to the limited number of proton-neutron configurations to mix, it is possible that effects due to subshell structures become apparent. This is especially true for the reduced transition probabilities $B(E2)$, which are much more sensitive to the particular composition of the wave functions of the nuclear states.

An interesting case is the evolution of the structure of the Po isotopes with $N \leqslant 126$. The two valence protons occupy the high-spin $0h_{9/2}$ orbital, which is fairly well isolated, while the lowest-lying valence neutron orbitals are $2p_{1/2}$, $1f_{5/2}$, and $2p_{3/2}$, which lie relatively close to each other. As a result, the low-lying structure of the Po isotopes close to the double-magic ^{208}Pb is dominated by the couplings of the two valence protons, forming a very-well pronounced seniority-scheme structure [4]. Seniority is the number of unpaired nucleons and usually for the higher-spin orbital could be considered as a good quantum number, and states can be labeled using it. In the case for the two-proton system, the seniority scheme manifests itself as a quintuple of states with spins 0^+, 2^+, 4^+, 6^+, and 8^+. The energy gap between the states decreases with spin, with 6^+ and 8^+ states being very close to each other, resulting in the 8^+ state being an isomer, which is a well established experimental fact. This picture persists down to ^{200}Po, where the 6^+ and 8^+ states begin to split in ^{198}Po (cf. Fig. 1 in Ref. [5]). While the excitation energies of the yrast states up to spin 8 could be described by the seniority scheme, the situation for the electromagnetic transition rates is not very clear, partly due to a lack of experimental data, especially between low-lying states. While the rates of the $8_1^+ \rightarrow 6_1^+$ transitions are low and evolve smoothly when moving away from the closed shell, recent lifetime measurements of the 4_1^+ states in ^{204,206}Po have revealed that there is an increase of the collectivity of the $4_1^+ \rightarrow 2_1^+$ transition when going from ^{206}Po to ^{204}Po [6]. The authors have also attempted to describe the structure of the two nuclei using a simple two-state mixing model that underestimates the $B(E2; 4_1^+ \rightarrow 2_1^+)$ values, pointing out the need for additional strength. This clearly necessitates the need for more sophisticated calculations.

One such approach can be shell-model calculations, with an interaction based on realistic nucleon-nucleon potential, which include all the valence orbitals for both protons and neutrons. Many such calculations have been performed for the open-shell nuclei with $N \geqslant 126$ and $Z \geqslant 82$ [7–12]. These calculations were based on the interaction of Kuo and Herling [13] and its modified version [9]. They were successful in describing the energy spectrum of the nuclei in the northwest of ^{208}Pb as well as in describing the static magnetic moments of some of the isomeric states of these nuclei.

Recently, the H208 interaction [14,15] was developed for the same region. The calculations with the newer H208 interaction gave a better agreement for the excitation energies. While there have been many large-scale shell-model calculations with interactions based on realistic nucleon-nucleon potentials performed for open-shell nuclei with $N \geqslant 126$, only recently have such calculations been performed for nuclei with $N \leqslant 126$. Furthermore, calculations were performed only for a limited number of nuclei. Successful calculations were performed for ^{209}Po [16] and ^{208}Po [17] using a residual interaction derived by means of the $\hat{Q}$ box folded-diagram

approach [18,19] which uses the CD-Bonn nucleon-nucleon potential [20] renormalized by the $V_{\mathrm{low}-k}$ approach [21]. In the paper of Brunet *et al.* [22] another approach was used where the proton-proton interaction and the neutron-neutron interaction were taken from Ref. [9] and the proton-neutron interaction was derived from the M3Y potential [23,24].

To shed more light on the evolution of electromagnetic rates of the even-even Po isotopes below $N \leqslant 126$, we present results on the lifetime measurements of the 2_1^+ and 4_1^+ states in ^{206}Po employing the recoil-distance Doppler-shift (RDDS) technique. We also present large-scale shell-model calculations for ^{204,206,208}Po aimed at describing the low-lying yrast states.

II. EXPERIMENT

The experiment was performed at the FN-Tandem accelerator of the University of Cologne. The nuclei of interest were populated in the ^{204}Pb(^{16}O, ^{14}C) ^{206}Po two-proton transfer reaction. An ^{16}O beam with an energy of 84 MeV and an average beam intensity of 1 pnA was delivered for 1 week on target. The target was a 0.6 mg/cm^2 ^{204}Pb layer evaporated on a 0.3 mg/cm^2 nat. V foil. The stopper used to stop the ejecting nuclei after the reaction induced on the target was a 2.0 mg/cm^2 natural V foil. The target and the stopper were stretched, parallel to each other, inside the Cologne plunger device [25]. Data were taken at seven target-to-stopper distances (1, 5, 10, 20, 50, 100, and 300 μm). Those distances are relative to a zero-offset distance of 37(12) μm determined using the capacitive method [25,26].

The γ rays produced in the experiment were detected by an array consisting of 11 high-purity germanium detectors placed in two rings at 45° and 142° around the plunger chamber. Recoiling light beamlike ions were detected by an array of six photovoltaic pin diodes, serving as a particle detector, placed at backward angles, covering angles between 120° and 165°. The γ-ray spectrum for the shortest plunger distance generated requiring at least one solar cell firing is show in Fig. 1(a). This spectrum is complex and contains a multitude of peaks of nuclei populated in the transfer reaction on the stopper, the target, and the backing of the target. Using a proper gate in the particle spectrum, corresponding to ^{14}C nuclei ejecting after reaction on the ^{204}Pb target, a γ-ray spectrum for the shortest plunger distance was generated and is displayed in Fig. 1(b). Due to the clean particle gate, predominantly transitions belonging to ^{206}Po are observed in the spectrum. Considerably weaker transitions belonging to ^{207,208}Po are also observed. A coincidence spectrum gated on the strongest $2_1^+ \rightarrow 0_1^+$ transition is displayed in Fig. 1(c). This spectrum further indicates the cleanness of the particle gate. Using the spectra for all the distances for both detector rings, together with the γ-gated spectrum, the γ intensities of the observed transition were measured. The relevant information on the observed γ transitions is summarized in Table I.

The RDDS data were analyzed by using the Bateman equations, using the method described in Ref. [25]. In this approach, the lifetime of a state of interest is determined using the quantity $R(t)$, which is defined as

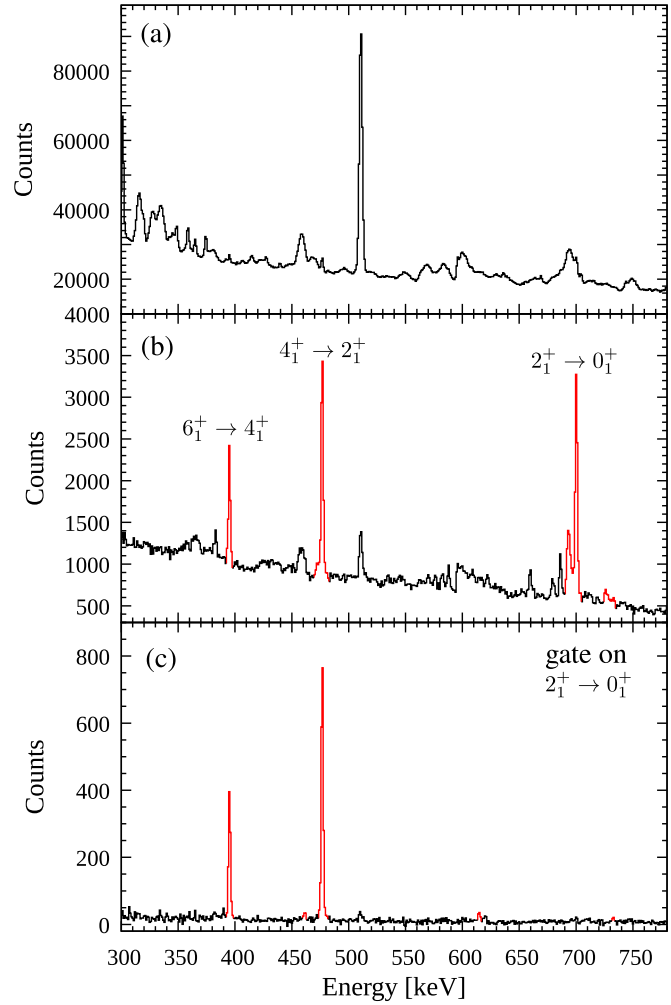

FIG. 1. (a) γ-ray spectrum of the backward detector ring taken at the shortest distance of 1 μm. (b) Particle-gated single γ-ray spectrum of the backward detector ring taken at the shortest distance of 1 μm. The strongest transitions belonging to ^{206}Po are indicated and colored in red. (c) Particle–gated γ-ray spectrum for all the distances of both detector rings.

TABLE I. γ-ray transitions observed in the ^{204}Pb(^{16}O, ^{14}C) ^{206}Po reaction. Transition intensities are normalized to the $2_1^+ \rightarrow 0_1^+$ transition. The spin assignments and the energies of the transitions are taken from the evaluated Nuclear Data Sheets [27]. The values for the energies have been rounded.

Transition	Energy (keV)	Intensity
$4_2^+ \rightarrow 4_1^+$	257	<2
$6_1^+ \rightarrow 4_1^+$	395	23.8(3)
$2_2^+ \rightarrow 2_1^+$	462	—[a]
$4_1^+ \rightarrow 2_1^+$	477	58.2(4)
$8_2^+ \rightarrow 8_1^+$	614	2.8(5)
$2_1^+ \rightarrow 0_1^+$	701	100.0(8)
$4_2^+ \rightarrow 2_1^+$	733	11.1(3)
$10_1^+ \rightarrow 8_1^+$	833	1.8(4)

[a]Could not be determined due to the presence of the $13/2_1^+ \rightarrow 9/2_1^-$ transition in ^{207}Po, which has an energy of 460 keV.

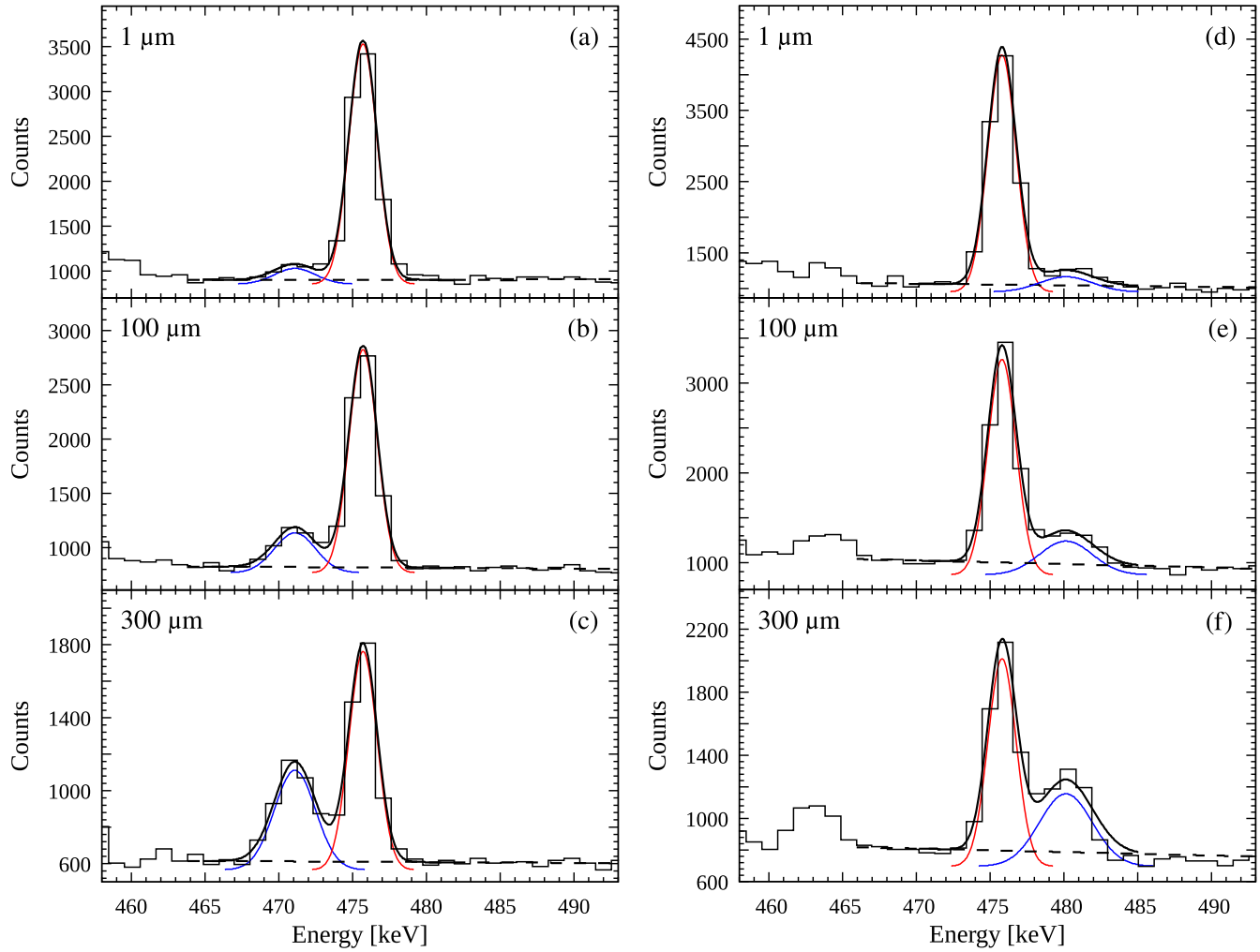

FIG. 2. [(a),(b),(c)] Fits to spectra of the backward detector ring for different target-to-stopper distances used to obtain the shifted and unshifted components of the $4_1^+ \rightarrow 2_1^+$ transition. The dashed black line represents the parametrization of the background used in the fit. The solid black line is the total fit to the spectrum. The red and blue Gaussians correspond to the shifted and the unshifted components, respectively. Panels (d), (e), and (f) are the same as panels (a), (b), and (c) but for the forward detector ring.

$R(t) = I_u(t)/[I_u(t) + I_s(t)]$, where $I_s(t)$ and $I_u(t)$ are the intensity of the shifted and the unshifted components of a transition that decays the excited state of interest. The ratio $R(t)$ is known as the decay curve and is a function of the time t after the nucleus was populated, which corresponds to the time of flight t of the excited ions between the target and the stopper. In the simple case where the state of interest has no feeders, the decay curve is an exponential decay with the reciprocal of the lifetime of the state τ being the decay constant $R(t) = e^{-t/\tau}$. In a realistic case, feeding is present, and it needs to be taken into account. The decay curve is then represented by a sum of different exponential functions. The coefficients before those exponential functions and the decay constants depend on the feeding lifetimes and feeding intensities. They are determined by solving a system of differential equations known as the Bateman equations [25]. The average speed of the recoiling ^{206}Po nuclei was determined by measuring the Doppler shift of the $2_1^+ \rightarrow 0_1^+$ and $4_1^+ \rightarrow 2_1^+$ transitions. The result of this procedure is $v = 1.17(5)\%$ c. This value was used to calculated the time of flight of the ^{206}Po nuclei between the stopper and the target for each of the distances.

The fits to the spectra for three selected target-to-stopper distances used to determine the lifetime of the 4_1^+ state are displayed in Fig. 2. The obtained $R(t)$ for both detector rings, together with the Bateman fit to them and the corresponding results for the lifetimes, are shown in Figs. 3(a) and 3(b). When performing the fit, the feeding coming from the higher-lying 4_2^+ and 6_1^+ states was taken into account. The $4_2^+ \rightarrow 2_1^+$ transition displays only a shifted component even at the lowest distance. It could be estimated that the effective lifetime of the 4_2^+ state is <5 ps, and the feeding coming from it could be considered as fast for the case of the 4_1^+ state. The $6_1^+ \rightarrow 4_1^+$ transition displays a very small shifted component only at the highest distance of 300 μm. It could be estimated that the effective lifetime of the 6_1^+ state is 2.1(5) ns. The quoted uncertainties of the lifetime of the 4_1^+ state, obtained using the two detector rings, were determined using a Monte Carlo

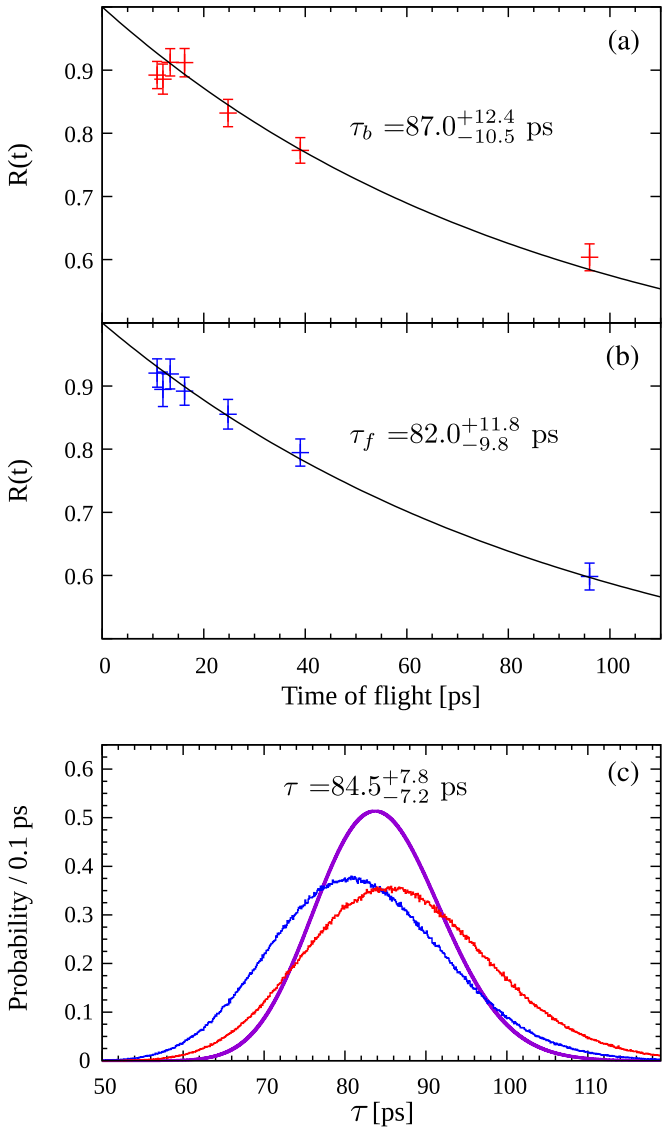

FIG. 3. (a) The experimentally obtained $R(t)$ ratios for the $4_1^+ \rightarrow 2_1^+$ transition for the backward detector ring together with the Bateman fit to the data points. (b) Same as panel (a) but for the forward detector ring. (c) Probability distributions for the fitted lifetimes obtained using a Monte Carlo procedure, as explained in the text, used to to determined the uncertainty of the measured lifetime. The blue and red distributions are for the forward and backward detector rings, respectively. The violet distribution is the convolution of the two distributions and is used to determine the final uncertainty of the lifetime of the 4_1^+ state.

procedure similar to the ones performed in Refs. [12,28]. In this procedure, the input parameters used in the Bateman fits are independently varied within the corresponding experimental uncertainties before performing the fit. This process is repeated a large number of times, and the results from each individual fit are written in a histogram displayed in Fig. 3(c). The value of the lifetime is determined as the statistical mean of the corresponding distribution, and the upper and the lower limits are determined as the σ_+ and σ_- intervals around the mean value. The final value for the 4_1^+ lifetime of $84.5^{+7.8}_{-7.2}$ ps is obtained from the convolution of the two distributions for the forward and backward detector rings. This lifetime is in good agreement with the lifetime of 89(7) ps obtained using the fast-timing method [6].

Using a similar procedure, the lifetime of the 2_1^+ state was obtained. The fits to the spectra are displayed in Fig. 4. The Bateman fits and the probability distributions are displayed in Fig. 5, where also the results are given. The delayed feeding coming from the 4_1^+ and 4_2^+ states is taken into account when performing the Batemans fit, whereas the feeding coming from the 2_2^+ state is short. The final result for the lifetime of the 2_1^+ state is $6.9^{+1.8}_{-1.6}$ ps. This result is consistent with the result of $3.8^{+2.9}_{-1.7}$ ps from Ref. [5], where the lifetime was determined based on a Coulomb excitation measurement. Here it is worth mentioning that the zero offset is rather large and has a big uncertainty, which makes this experiment not optimal for measuring short lifetimes. Using the measured lifetimes of the 2_1^+ and 4_1^+ states, the $B(E2; 2_1^+ \rightarrow 0_1^+) = 686^{+211}_{-150}\ e^2\ \mathrm{fm}^4$ and $B(E2; 4_1^+ \rightarrow 2_1^+) = 378^{+35}_{-32}\ e^2\ \mathrm{fm}^4$ values were calculated.

III. DISCUSSION

To interpret the results, large-scale shell-model calculations were performed. The calculations were performed without truncations, in a basis containing the orbitals $0h_{9/2}$, $1f_{7/2}$, $0i_{13/2}$, $1f_{5/2}$, $2p_{3/2}$, and $2p_{1/2}$, for both protons and neutrons. The two-body matrix elements (TBMEs) were taken from Ref. [9] for the proton-proton and neutron-neutron parts of the interaction. The proton-neutron part was taken from Ref. [29] where the TBMEs were obtained using the G-matrix approach with a MY3 nucleon-nucleon interaction. A similar approach was recently used to describe the structure of ^{208}Po [22]. The effective single-particle energies were adjusted to reproduce the excitation spectrum of the ^{209}Bi and ^{207}Pb nuclei. The results for the yrast-state energies up to spin 8 for ^{204,206,208}Po are labeled as SM1 and are presented in Table II. The calculations describe well the energies of the first excited 2^+ and 4^+ states as well as the staggering of the levels when going up the band, especially the very small gap between the 6_1^+ and 8_1^+ states. The calculations, however, predict that the energy gap between the 4_1^+ and 6_1^+ states is smaller than the experimentally observed one, which results in an underprediction of the absolute excitation energies of the 6_1^+ and 8_1^+ states. This problem becomes more apparent when going toward the lighter Po isotopes.

The electric quadrupole moment Q and $E2$ strengths were calculated using the effective charges $e_\pi = 1.5\ e$ and $e_\nu = 0.85\ e$. Please note that no attempt was made to make a global fit for the effective charges, and their values are given as a reference. The results of the calculations for the quadrupole moments of the 8_1^+ states are labeled as SM1 and are given in Table III. The calculations describe well the experimentally available data, albeit being slightly lower, which could be easily compensated by increasing e_π. The calculations also describe some of the available data on the $B(E2)$ values within the yrast band with a notable exception of the $B(E2; 4_1^+ \rightarrow 2_1^+)$ value in ^{208}Po and the $B(E2; 4_1^+ \rightarrow 2_1^+)$ and $B(E2; 6_1^+ \rightarrow 4_1^+)$ values in ^{206}Po.

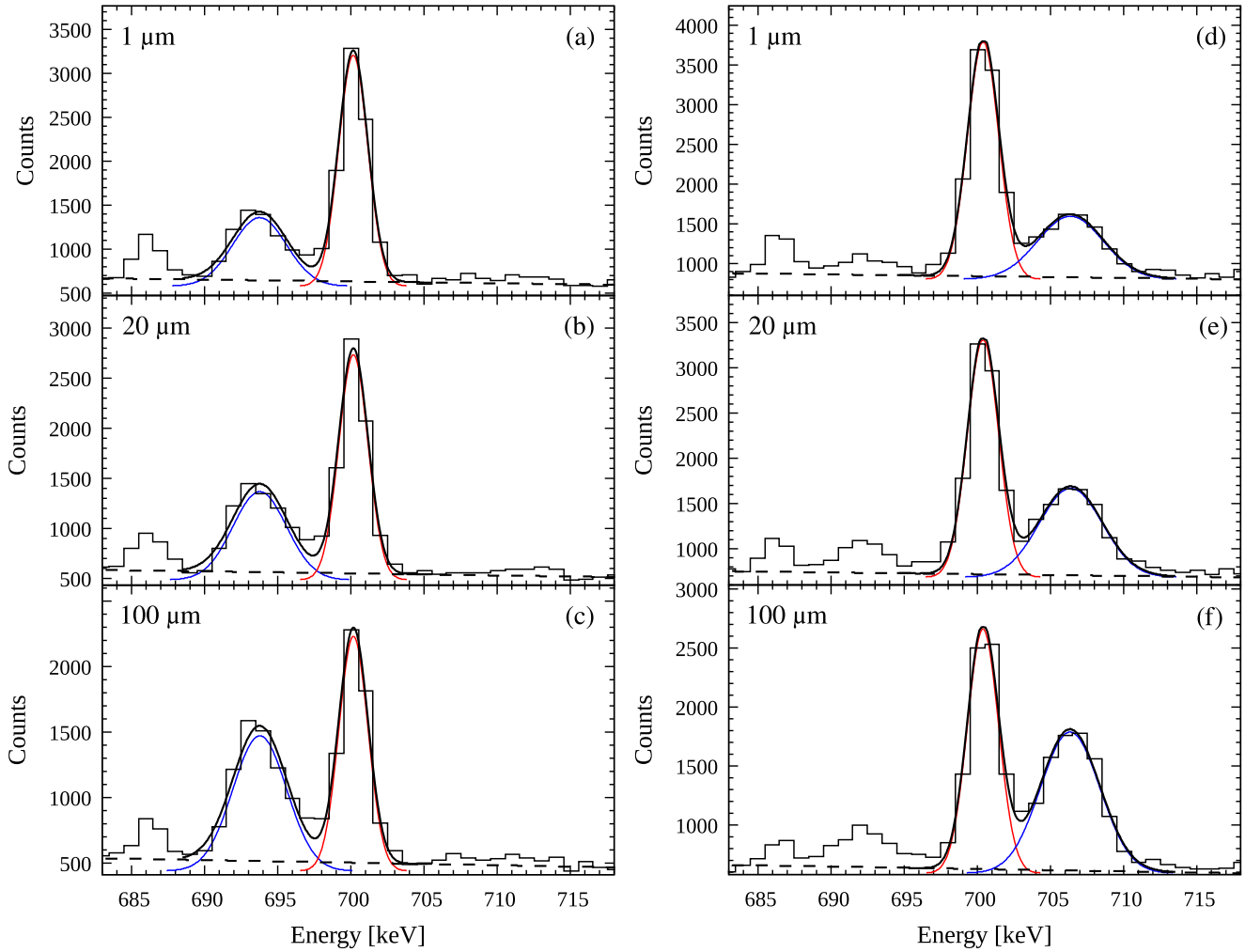

FIG. 4. Same as Fig. 2 but for the $2_1^+ \rightarrow 0_1^+$ transition and distances of 1, 20, and 100 μm.

This could be related to the fact that the structure of the 2_1^+ and/or 4_1^+ state cannot be described fully by the shell-model calculations performed. In an attempt to resolve the problem, adjustments were made to the two-body matrix elements of the proton-neutron interaction involving the $\pi 0h_{9/2}$, $\nu 2p_{3/2}$, and $\nu 2p_{1/2}$ orbitals—the values of $\langle 0\pi h_{9/2}, 2\nu p_{3/2}|\hat{V}|0\pi h_{9/2}, 2\nu p_{3/2}\rangle_{J=5}$, $\langle 0\pi h_{9/2}, 2\nu p_{1/2}|\hat{V}|0\pi h_{9/2}, 2\nu p_{1/2}\rangle_{J=4}$, and $\langle 0\pi h_{9/2}, 2\nu p_{1/2}|\hat{V}|0\pi h_{9/2}, 2\nu p_{1/2}\rangle_{J=5}$ were deceased by 0.10 MeV. The new results are designated as SM2 and are given in Tables II and III as well as in Fig. 6. The SM2 calculations give a considerably better reproduction of the $B(E2)$ values for the yrast states while having a minimal effect on the calculated quadrupole moments. The new calculations also predict lower energies for all the yrast states, which on the one hand, improves the reproducibility for the 2_1^+ and 4_1^+ state energies. However, on the other hand, the calculated 6_1^+ and 8_1^+ states are further lowered than the experimental values. The $B(E2; 4_1^+ \rightarrow 2_1^+)$ value in ^{208}Po is still overpredicted, albeit the calculated value is much closer to the experimental one. Of interest here is that the authors of Ref. [17], in an attempt to describe the $M1$ strength of the $2_2^+ \rightarrow 2_1^+$ transition in ^{208}Po, have introduced a similar adjustment of the values of the $\langle 0\pi h_{9/2}, 2\nu p_{1/2}|\hat{V}|0\pi h_{9/2}, 2\nu p_{1/2}\rangle_{J=4}$ and $\langle 0\pi h_{9/2}, 2\nu p_{1/2}|\hat{V}|0\pi h_{9/2}, 2\nu p_{1/2}\rangle_{J=5}$ two-body matrix elements. Here it could be noted that the $B(E2; 4_1^+ \rightarrow 2_1^+)$ value does not fit the generally established trends and has a value lower than the one in the neighboring ^{210}Po, which is a semimagic nucleus. It would be important to remeasure the lifetime of the 4_1^+ state in ^{208}Po to conclude whether the $B(E2; 4_1^+ \rightarrow 2_1^+)$ value is indeed unexpectedly low. This lifetime is also an important input parameter when determining the lifetime of the 2_1^+ state. One such measurement can be done using the fast-timing technique after the electron capture decay of ^{208}At.

Magnetic moments and $M1$ transition rates for ^{204,206,208}Po were calculated using the effective g factors $g_s^\pi = 3.54$ and $g_l^\pi = 1.13$ for the protons and $g_s^\nu = -2.03$ and $g_l^\nu = -0.08$ for the neutrons. Those g factors were introduced by Arima *et al.* [30] to account for core polarization and mesonic-exchange currents in nuclei in the ^{208}Pb region. Recently, these g factors with the same interactions were used to suc-

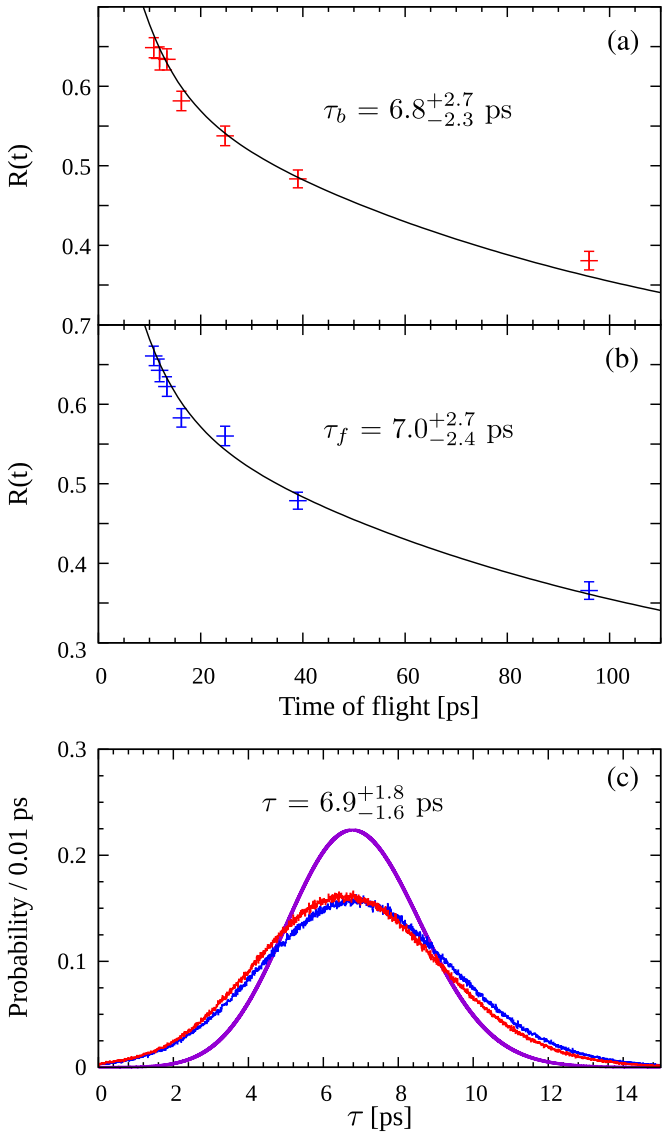

FIG. 5. Same as Fig. 3 but the analysis was performed for the $2_1^+ \rightarrow 0_1^+$ transition and results are for the 2_1^+ state.

cessfully calculate magnetic moments in $N = 126$ isotopes [31] as well as the $B(M1; 7/2_2^- \rightarrow 7/2_1^-)$ value in ^{211}At [28]. The results from the current calculations (SM1 and SM2) are given in Table IV. It can be seen that the SM1 and SM2 calculations give very similar results for the magnetic moments, which both describe very well the available experimental data. Additionally, the relatively high $M1$ strength of the $2_2^+ \rightarrow 2_1^+$ transition in ^{208}Po is also described by the SM2 calculations, albeit being slightly lower than the experimental value obtained in Ref. [32]. The SM1 calculation overpredicts the $B(M1; 2_2^+ \rightarrow 2_1^+)$ value but not significantly. Here it is worth mentioning that in Ref. [17], shell-model calculations within the same valence space were performed for ^{208}Po. Those calculations gave a good description of the yrast states and their $E2$ transition strengths. However, a modification had to be made to some two-body matrix elements so the $B(M1; 2_2^+ \rightarrow 2_1^+)$ value could be described, which results in a very high energy of the 2_1^+ state. It will be of great interest to see how these calculations describe the properties of the lighter Po isotopes and whether they better describe the energies of the 6_1^+ and 8_1^+ states.

In conclusion, the shell-model calculations presented here describe the key features of yrast states of ^{204,206,208}Po isotopes, including the observed enhanced $M1$. The introduced modification to the interaction improves the reproducibility of the transition rates. Unfortunately, the calculations underpredict the energies of 6_1^+ and 8_1^+. This problem could be possibly addressed by making more modifications to the proton-neutron interaction.

IV. CONCLUSION AND OUTLOOK

The lifetimes of the 2_1^+ and 4_1^+ states in ^{206}Po were measured using the RDDS technique. The deduced reduced transition probabilities are compared to large-scale shell-model calculations performed for ^{204,206,208}Po. The calculations describe well the $E2$ strengths within the yrast bands of the ^{204,206,208}Po isotopes with the only exception of the $4_1^+ \rightarrow 2_1^+$ transition in ^{208}Po. The calculations also describe the enhanced $M1$ strength of the $2_2^+ \rightarrow 2_1^+$ transition in ^{208}Po. However, the calculations underpredict the values of the 6_1^+ and 8_1^+ energies, which suggests that further empirical adjustment to the two-body matrix element might be necessary to improve the reproducibility for the energies of the states. It will be of interest to continue the experimental studies of the transition rates of the nuclei in the region northwest of ^{208}Pb.

TABLE II. Observed and calculated energies for yrast states in ^{204,206,208}Po. The experimental data are taken from the evaluated nuclear data sheets [27,33,34] and rounded.

	Energy (keV)								
	^{204}Po			^{206}Po			^{208}Po		
State	Expt.	SM1	SM2	Expt.	SM1	SM2	Expt.	SM1	SM2
2_1^+	684	769	737	701	760	721	687	724	707
4_1^+	1201	1235	1204	1162	1222	1201	1347	1357	1376
6_1^+	1627	1478	1417	1573	1462	1386	1524	1472	1456
8_1^+	1639	1497	1433	1586	1480	1400	1528	1477	1480

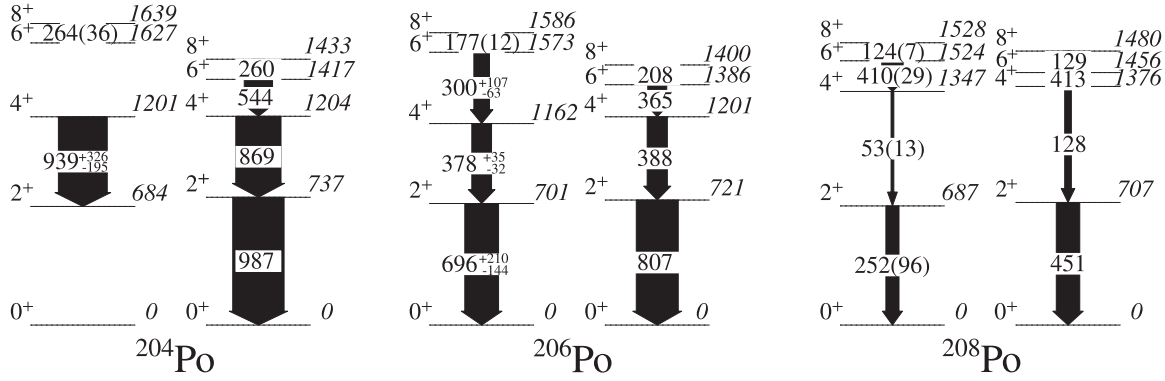

FIG. 6. Comparison of experimental (left) low-lying yrast states of ^{204,206,208}Po with the shell-model calculations SM2 (right). Data are from Tables II and III. The width of the arrows are proportional to the absolute $E2$ transition strengths between the states. The numbers over the arrows are the reduced $E2$ transition probabilities in e^2 fm^4. The positions of the 8^+ states have been elevated by 100 keV to make the transition strength value to the 6_1^+ state clearly visible.

TABLE III. Observed and calculated $E2$ transition rates and quadrupole moments Q for yrast states in ^{204,206,208}Po. The experimental data are taken from the evaluated Nuclear Data Sheets [27,33,34], unless otherwise mentioned.

	$B(E2)$ (e^2 fm^4)								
	^{204}Po			^{206}Po			^{208}Po		
Transition	Expt.	SM1	SM2	Expt.	SM1	SM2	Expt.	SM1	SM2
$2_1^+ \to 0_1^+$	—	983	987	686^{+211}_{-150}[b]	788	807	252(96)[d]	512	451
$4_1^+ \to 2_1^+$	939^{+326}_{-195}[a]	749	869	378^{+35}_{-32}[b]	145	388	53(13)[d]	409	128
$6_1^+ \to 4_1^+$	—	453	544	300^{+107}_{-63}[c]	178	365	410(29)	442	413
$8_1^+ \to 6_1^+$	264(36)	262	260	177(12)	212	208	124(7)[e]	127	129
State				Q (e fm^2)					
2_1^+	114(5)	102	102	102(4)	94	95	90(4)	88	85

[a]From Ref. [6].
[b]From this work.
[c]From Ref. [35].
[d]From Ref. [17].
[e]Value calculated using the lifetime from Ref. [34] and revised conversion coefficient of 3.3×10^6 obtained by Ref. [36] and calculated according to Ref. [37].

The results of those studies will serve as an important input for future theoretical calculations.

ACKNOWLEDGMENTS

V.K. thanks B. A. Brown from MSU for providing the interaction TBMEs used in the calculations presented here. We are thankful to Andrey Blazhev from IKP, Cologne, for making the target used in this experiment. This material is based upon work supported by the U.S. Department of Energy, Office of Science, Office of Nuclear Physics, under Contract No. DE-AC02-06CH11357 (ANL).

TABLE IV. Observed and calculated magnetic moments μ and reduced B(M1) transition probabilities, using effective g factors $g_s^\pi = 3.54$ and $g_l^\pi = 1.13$ for the protons and $g_s^\nu = -2.03$ and $g_l^\nu = -0.08$ for the neutrons.

		μ (μ_N)		
Nucleus	State	Expt.	SM1	SM2
^{208}Po	8^+	7.37(5)[a]	7.26	7.25
	6^+	5.3(6)[a]	5.37	5.39
^{204}Po	8^+	7.38(10)[b]	7.15	7.14
Nucleus	Transition	B(M1) (μ_N^2)		
^{208}Po	$2_2^+ \to 2_1^+$	$\geqslant 0.116(14)$[c]	0.161	0.093

[a]From Nuclear Data Sheets for $A = 208$ [34].
[b]From Nuclear Data Sheets for $A = 204$ [33].
[c]From Ref. [32].

[1] B. B. Mottelson, in *Proceedings of the International School of Physics "Enrico Fermi," Course XV, Vaxenna, 1960*, edited by G. Racah (Academic, London, 1960), Vol. 329, p. 44.
[2] P. Federman and S. Pittel, Phys. Rev. C **20**, 820 (1979).
[3] R. Casten, Nucl. Phys. A **443**, 1 (1985).
[4] I. Talmi, Nucl. Phys. A **172**, 1 (1971).
[5] T. Grahn *et al.*, Eur. Phys. J. A **52**, 340 (2016).
[6] M. Stoyanova *et al.*, Phys. Rev. C **100**, 064304 (2019).
[7] J. McGrory and T. Kuo, Nucl. Phys. A **247**, 283 (1975).
[8] T. R. McGoram, G. Dracoulis, A. Byrne, A. Poletti, and S. Bayer, Nucl. Phys. A **637**, 469 (1998).
[9] E. K. Warburton and B. A. Brown, Phys. Rev. C **43**, 602 (1991).
[10] L. Coraggio, A. Covello, A. Gargano, N. Itaco, and T. T. S. Kuo, Phys. Rev. C **58**, 3346 (1998).
[11] E. Caurier, M. Rejmund, and H. Grawe, Phys. Rev. C **67**, 054310 (2003).
[12] V. Karayonchev, G. Rainovski, J. Jolie, A. Blazhev, A. Dewald, A. Esmaylzadeh, C. Fransen, P. John, L. Knafla, D. Kocheva, K. Schomacker, V. Werner, and H. Naïdja, Phys. Rev. C **106**, 064305 (2022).
[13] G. Herling and T. Kuo, Nucl. Phys. A **181**, 113 (1972).
[14] H. Naïdja, Phys. Scr. **94**, 014005 (2019).
[15] H. Naïdja, Phys. Rev. C **103**, 054303 (2021).
[16] V. Karayonchev, M. Stoyanova, G. Rainovski, J. Jolie, A. Blazhev, M. Djongolov, A. Esmaylzadeh, C. Fransen, K. Gladnishki, L. Knafla, D. Kocheva, L. Kornwebel, J.-M. Régis, G. De Gregorio, and A. Gargano, Phys. Rev. C **103**, 044309 (2021).
[17] D. Kalaydjieva, D. Kocheva, G. Rainovski, V. Karayonchev, J. Jolie, N. Pietralla, M. Beckers, A. Blazhev, A. Dewald, M. Djongolov, A. Esmaylzadeh, C. Fransen, K. A. Gladnishki, A. Goldkuhle, C. Henrich, I. Homm, K. E. Ide, P. R. John, R. Kern, and J. Kleemann, Phys. Rev. C **104**, 024311 (2021).
[18] L. Coraggio, A. Covello, A. Gargano, N. Itaco, and T. Kuo, Prog. Part. Nucl. Phys. **62**, 135 (2009).
[19] L. Coraggio, A. Covello, A. Gargano, N. Itaco, and T. Kuo, Ann. Phys. **327**, 2125 (2012).
[20] R. Machleidt, Phys. Rev. C **63**, 024001 (2001).
[21] S. Bonger, T. Kuo, and L. Coraggio, Nucl. Phys. A **684**, 432 (2001).
[22] M. Brunet *et al.*, Phys. Rev. C **103**, 054327 (2021).
[23] W. G. Love, *The (p,n) Reaction and the Nucleon-Nucleon Force* (Springer, Boston, 1980), p. 23.
[24] G. Bertsch, J. Borysowicz, H. McManus, and W. Love, Nucl. Phys. A **284**, 399 (1977).
[25] A. Dewald, O. Möller, and P. Petkov, Prog. Part. Nucl. Phys. **67**, 786 (2012).
[26] T. Alexander and A. Bell, Nucl. Instrum. Methods **81**, 22 (1970).
[27] F. Kondev, Nucl. Data Sheets **109**, 1527 (2008).
[28] V. Karayonchev, A. Blazhev, J. Jolie, A. Dewald, A. Esmaylzadeh, C. Fransen, G. Häfner, L. Knafla, C. Müller-Gatermann, G. Rainovski, J.-M. Régis, K. Schomacker, and P. Van Isacker, Phys. Rev. C **106**, 044321 (2022).
[29] B. A. Brown, Phys. Rev. Lett. **85**, 5300 (2000).
[30] A. Arima, K. Shimizu, W. Bentz, and H. Hyuga, *Advances in Nuclear Physics*, edited by E. V. W. Negele (Plenum, New York, 1987), Vol. 18.
[31] V. Karayonchev, A. Blazhev, A. Esmaylzadeh, J. Jolie, M. Dannhoff, F. Diel, F. Dunkel, C. Fransen, L. M. Gerhard, R.-B. Gerst, L. Knafla, L. Kornwebel, C. Müller-Gatermann, J.-M. Régis, N. Warr, K. O. Zell, M. Stoyanova, and P. Van Isacker, Phys. Rev. C **99**, 024326 (2019).
[32] A. Yaneva *et al.*, Eur. Phys. J. A **56**, 246 (2020).
[33] C. Chiara and F. Kondev, Nucl. Data Sheets **111**, 141 (2010).
[34] M. Martin, Nucl. Data Sheets **108**, 1583 (2007).
[35] K. Stoychev, M. Djongolov, V. Karayonchev, G. Rainovski, M. Ley, J. Jolie, D. Bittner, A. Blazhev, F. Dunkel, A. Esmaylzadeh, C. Fransen, J. Garbe, L. M. Gerhard, R.-B. Gerst, K. Geusen, K. A. Gladnishki, G. Häfner, D. Kalaydjieva, L. Klöckner, and L. Knafla, Phys. Rev. C **108**, 014316 (2023).
[36] T. Kibédi (private communication).
[37] T. Kibédi, T. Burrows, M. Trzhaskovskaya, P. Davidson, and C. W. Nestor, Nucl. Instrum. Methods Phys. Res. Sect. A **589**, 202 (2008).